Proceedings of the 17th World Congress
The International Federation of Automatic Control
Seoul, Korea, July 6-11, 2008

Fixed-Point DSP Implementation of Nonlinear H_∞ Controller for Large Gap Electromagnetic Suspension System

Paulo H. da Rocha * **Henrique C. Ferreira** **
Michael C. Porsch * **Roberto M. Sales** **

* *Centro Tecnológico da Marinha em São Paulo, Electro-Electronic Project Division, Av. Prof. Lineu Prestes, n. 2468, CEP 05508-000, São Paulo (SP), Brazil*
(e-mail: ph_rocha@yahoo.com, michaelcp@bol.com.br)

** *University of São Paulo, Department of Telecommunication and Control Engineering, Av. Prof. Luciano Gualberto, trv. 3, n. 158, CEP 05508-900, São Paulo (SP), Brazil*
(e-mail: henrique@lac.usp.br, roberto@lac.usp.br)

Abstract: Electromagnetic suspension systems are inherently nonlinear and, when digitally controlled, frequently face hardware limitations. The main contributions of this paper are: the design of a nonlinear H_∞ controller, including dynamic weighting functions for such a system and the presentation of a practical procedure to implement this controller on a fixed-point DSP. Experimental results are also presented, in which the performance of the nonlinear controller is evaluated specifically in the initial suspension phase, when the starting gap is too far from the equilibrium working gap.

Keywords: Digital implementation; Embedded systems; Digital signal processors; Magnetic bearings; Word length; H-infinity control; Robust control; Nonlinear control systems.

1. INTRODUCTION

Electromagnetic Suspension Systems (ESS) have been widely used and studied, specially because magnetic actuators present some advantages over other types of actuators, such as non-contact actuation, avoiding mechanical wear. These systems are inherently nonlinear and open-loop unstable, and the development of high performance position controllers for levitated objects motivated the publishing of many papers along the last decade (Bleuler, 1992; Nadashima, 1994; Bittar and Sales, 1998).

However, most of the papers presented focused on models obtained by means of linearization of the system at nominal working gap and were not concerned about instability during suspension phase, specially when there are large initial gaps. Some papers approached the subject of varying linear plant according to the gap by switching controllers (Al-Muthairi and Zribi, 2004; Banerjee et al., 2006).

This work presents a practical control system design strategy and experimental results. The process starts from a H_∞ controller for a linearized plant around a nominal gap. Then, the same weighting functions are used in the design of a nonlinear H_∞ controller. The use of weighting functions with dynamics in nonlinear H_∞ controls systems has not been used in similar works, which explore only static weighting functions (Sinha and Pechev, 2004). In this way, it was possible to operate with large starting gaps with better results than those obtained by linear H_∞ control design.

In addition, this work presents some practical aspects of hardware and firmware implementation of the controller and a procedure for determining the required word length in a DSP using the fixed-point ToolBox from MATLAB and IQMath Library from Texas Instruments.

2. SYSTEM MODELING

In the ESS shown in Fig. 1, the electrical current $i(t)$ through the magnetic coil actuator generates the attraction force $F(t)$ on the payload with mass m; $x(t)$ represents the air-gap and g the local gravity acceleration. The vertical dynamic mathematical model is described by (1):

$$m\ddot{x}(t) = mg - F(t), \tag{1}$$

and the attractive force is given by (Sinha, 1987; Bittar and Sales, 1998):

$$F(t) = k\frac{i(t)^2}{x(t)^2}, \tag{2}$$

where k is the magnetic actuator constant, which depends on the bearing geometry and electrical characteristics.

In the equilibrium condition, $\ddot{x} = 0$,

$$k\frac{i_0^2}{x_0^2} = mg, \tag{3}$$

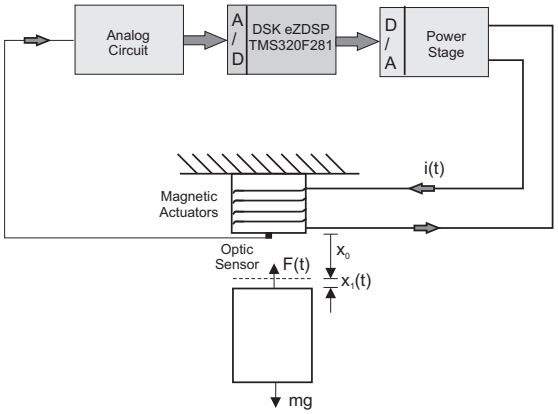

Fig. 1. Block diagram of ESS

Table 1. Prototype characteristic

equilibrium gap	$x_0 = 5$mm
equilibrium current	$i_0 = 380$mA
bearing constant	$k = 1.6 \cdot 10^{-4}\text{Nm}^2/\text{A}^2$
power stage constant	$k_{pot} = 0.25\text{V/A}$
mass	$m = 0.240$kg

where x_0 and i_0 are position and current in the equilibrium point, respectively. Considering small disturbances $x_\delta(t)$ and $i_\delta(t)$ around the equilibrim point (x_0, i_0), the linearization of (1) gives

$$m\ddot{x}_\delta(t) = \frac{2ki_0^2}{x_0^3}x_\delta(t) - \frac{2ki_0}{x_0^2}i_\delta(t). \tag{4}$$

Combining (3) and (4), gives

$$\ddot{x}_\delta(t) = \frac{2g}{x_0}x_\delta(t) - \frac{2g}{i_0}i_\delta(t). \tag{5}$$

As shown in section 4.1, the electronic power circuit is designed so that the relationship between the control voltage and the magnet coil current is linear, as expressed in (6) and (7)

$$v_\delta(t) = -k_{pot}i_\delta(t), \tag{6}$$

$$x_\delta(t) = k_s x_\delta^{(v)}(t), \tag{7}$$

where $v_\delta(t)$ and $x_\delta^{(v)}(t)$ are small disturbances around the equilibrium point. k_{pot} and k_s are constants defined in the hardware setup.

Replacing (6) and (7) in (5) gives

$$\ddot{x}_\delta^{(v)}(t) = \frac{2g}{x_0}x_\delta^{(v)}(t) + \frac{2g}{k_{pot}k_s i_0}v_\delta(t). \tag{8}$$

The following open-loop system transfer function is obtained from (8):

$$G(s) = \frac{X_\delta^{(v)}(s)}{V_\delta(s)} = \frac{\frac{2g}{k_{pot}k_s i_0}}{\left(s + \sqrt{\frac{2g}{x_0}}\right)\left(s - \sqrt{\frac{2g}{x_0}}\right)}. \tag{9}$$

Table 1 presents some prototype characteristics.

3. CONTROLLER DESIGN PROCEDURE

The controller design procedure presented in this section follows the same lines of (Sinha and Pechev, 2004). The main difference lies on the fact that, similarly to the linear H_∞ control practice, dynamic weighting functions are here explored with robustness purposes.

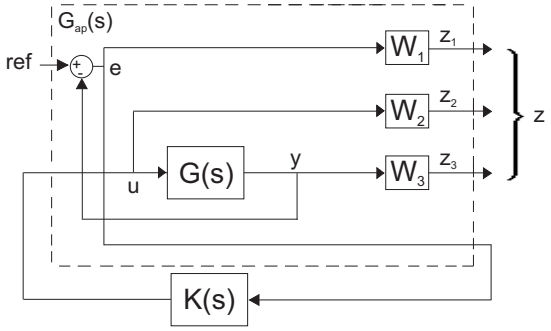

Fig. 2. Block diagram for the control system design

3.1 Dynamic Weighting Functions Specification

The methodology for specifying of weighting functions in the case of linear H_∞ control design is well established in the literature (Doyle et al., 1989). However, in the case of nonlinear H_∞ control design, only static weighting functions have been evaluated (Sinha and Pechev, 2004), although, from a theoretical point of view, it can be easily shown that dynamic weighting functions may also be included in the design (Isidori and Astolfi, 1992). Fig. 2 presents the standard block diagram for the control system including the plant, the controller and the weighting functions.

In this section, the nonlinear plant shown in (8) is firstly linearized around the operation gap, as in section 2. Then dynamic weighting functions

$$W_1(s) = \frac{20}{s + 0.4} \tag{10}$$

related to performance robustness, and

$$W_3(s) = 20\frac{s + 0.045}{s + 3000} \tag{11}$$

related to noise attenuation and uncertainty robustness are specified in the context of the linear H_∞ control design. In order to simplify, the weighting function $W_2(s)$, related to the control signal, is assumed to be equal to the unit.

In the next section, these weighting functions will be included in the nonlinear H_∞ design.

3.2 Nonlinear H_∞ Output Feedback Control Design

Observing the EES represented in Fig. 1, combing (1) and (2) and defining $x_1 = x - x_0$, $x_2 = \dot{x}$, $\bar{x}_1 = x_0$, $u = (i - i_0)^2$ with i_0 as in (3), the nonlinear state space model can be expressed as

$$\begin{aligned} \dot{x}_1 &= x_2, \\ \dot{x}_2 &= g - g\frac{\bar{x}_1^2}{(\bar{x}_1 + x_1)^2} - \frac{k}{m}\frac{u}{(\bar{x}_1 + x_1)^2} + \frac{1}{m}w_1, \\ y &= x_1 + w_2, \end{aligned} \tag{12}$$

where w_1 represents the external force disturbance, while w_2 represents the noise acting on the plant. Equation (12) can be rewritten as

$$\begin{aligned} \dot{x}_p &= f_p(x_p) + g_{p1}(x_p)w + g_{p2}(x_p)u, \\ y &= h_{p2}(x_p) + k_{p21}(x_p)w, \end{aligned} \tag{13}$$

where

$$f_p(x) = \begin{bmatrix} x_2 \\ g - g\dfrac{\bar{x}_1^2}{(\bar{x}_1 + x_1)^2} \end{bmatrix}, \quad g_{p1}(x) = \begin{bmatrix} 0 & 0 \\ \dfrac{1}{m} & 0 \end{bmatrix},$$
$$g_{p2}(x) = \begin{bmatrix} 0 \\ -\dfrac{k}{m}\dfrac{1}{(\bar{x}_1 + x_1)^2} \end{bmatrix}, \quad h_{p1}(x) = \begin{bmatrix} x_1 \\ x_2 \\ 0 \end{bmatrix},$$
$$k_{p11}(x) = 0, \quad k_{p12}(x) = [\,0 \;\; 0 \;\; 1\,]^T,$$
$$h_{p2}(x) = x_1, \quad k_{p21} = [\,0 \;\; 1\,].$$

The dynamic weighting functions (10) and (11) can be expressed, in state space form, as:

$$\begin{aligned} \dot{x}_{w1} &= A_{w1}x_{w1} + B_{w1}(h_{p2}(x_p) + k_{p21}(x_p)w), \\ z_1 &= C_{w1}x_{w1}, \\ \dot{x}_{w3} &= A_{w3}x_{w3} + B_{w3}h_{p2}(x_p), \\ z_3 &= C_{w3}x_{w3} + D_{w3}h_{p2}(x_p), \end{aligned} \tag{14}$$

Moreover,

$$z_2 = W_2 u, \tag{15}$$

where W_2 is a constant, in order to simplify.

Combining (13), (14) and (15), we have

$$\begin{aligned} \dot{x} &= f(x) + g_1(x)w + g_2(x)u, \\ z &= h_1(x) + k_{11}w + k_{12}u, \\ y &= h_2(x) + k_{21}(x)w, \end{aligned} \tag{16}$$

where

$$x = \begin{bmatrix} x_p \\ x_{w1} \\ x_{w3} \end{bmatrix}, \quad f(x) = \begin{bmatrix} f_p(x_p) \\ A_{w1}x_{w1} + B_{w1}h_{p21}(x_p) \\ A_{w3}x_{w3} + D_{w3}h_{p2}(x_p) \end{bmatrix},$$
$$g_1(x) = \begin{bmatrix} g_{p1}(x_p) \\ B_{w1}k_{p21}(x_p) \\ 0 \end{bmatrix}, \quad g_2(x) = \begin{bmatrix} g_{p2}(x_p) \\ 0 \\ 0 \end{bmatrix},$$
$$h_1(x) = \begin{bmatrix} C_{w1}x_{w1} \\ 0 \\ C_{w3}x_{w3} + D_{w3}h_{p2}(x_p) \end{bmatrix}, \quad k_{11}(x) = \begin{bmatrix} 0 \\ 0 \\ 0 \end{bmatrix},$$
$$k_{12}(x) = \begin{bmatrix} 0 \\ W_2 \\ 0 \end{bmatrix}, \quad h_2(x) = h_{p2}(x_p), \quad k_{21}(x) = k_{p21}(x_p).$$

The nonlinear H_∞ project purpose is to find a class of admissible controllers with local attenuation of the exogenous input that satisfies the L_2-gain inequality (van der Schaft, 1992)

$$\int_0^T \|z(t)\|^2 dt \le \gamma^2 \int_0^T \|w(t)\|^2 dt, \quad \gamma \ge 1 \tag{17}$$

where $z(t)$ is the penalty vector and $w(t)$ is the disturbance input vector, as shown in Fig. 2. The equilibrium point of a dissipative dynamical system is stable if for $x(t) = 0|_{t=0}$ there is a nonnegative smooth storage function V(x(t)) that satisfies the Hamilton-Jacobi-Isaacs (HJI) inequality (Isidori and Astolfi, 1992).

$$\begin{aligned} &V_x^T(f(x) + g_1(x)w + g_2(x)u) + L(x,w,u) \le 0 \\ &L(x,w,u) = h_1^T h_1 + \|u\|^2 - \gamma^2\|w\|^2 \end{aligned} \tag{18}$$

where $V_x = \partial V(x(t))/\partial x(t)$. The left-hand side of the HJI inequality is known as the Hamiltonian function $H(x, V(x), w, u)$. The goal of the design procedure is to find $u(x)$ that satisfies the HJI inequality. The analytical derivations are focused on finding a saddle point in the Hamiltonian function so that

$$H(x, V_x, w, u_*) \le H(x, V_x, w_*, u_*) \le H(x, V_x, w_*, u), \tag{19}$$

where w_* is the worst disturbance input that maximizes the Hamiltonian and u_* is the control input law that minimizes the Hamiltonian. With $k = k_{12}^T k_{12} = I$ and $h_1^T k_{12} = 0$, w_* and u_* can be defined as (van der Schaft, 1992; Isidori and Astolfi, 1992)

$$w_* = \frac{1}{2\gamma^2} g_1^T V_x^T, \quad u_* = -\frac{1}{2} g_2^T V_x^T. \tag{20}$$

So as to determine the storage function $V(x(t))$ that satisfies the saddle point condition, (20) is translated into (18), thus the following HJI inequality can be defined as:

$$\begin{aligned} H_*(x, V_x) = {} & V_x^T f + h_1^T h_1 + \frac{1}{4\gamma^2} V_x g_1 g_1^T V_x^T \\ & -\frac{1}{4} V_x g_2 g_2^T V_x^T \le 0. \end{aligned} \tag{21}$$

Due to the difficulty in finding an analytic solution for this equation, (21) is converted into an infinite sum inequality by Taylor's series. Using this numerical approximation, with the ESS parameters defined in Table 1, the corresponding first-order control law is then given by

$$u = 4796.2x_1 + 125.52x_2 + 1711.5x_3 - 1038.2x_4. \tag{22}$$

Once the state variable $x_2(t)$ is not available for feedback control in the ESS, a state estimator in conjunction with the control law is designed. The state variables $x_3(t)$ and $x_4(t)$ are calculated by the filters $W_1(s)$ and $W_3(s)$, respectively. The nonlinear estimator was obtained using the concept of local dissipation presented in (Isidori and Kang, 1995). Considering the system below

$$\begin{aligned} \dot{\bar{x}} &= f(\bar{x}) + g_1(\xi)w(\bar{x}) + g_2(\bar{x})u(\bar{x}) + G(\bar{x})(y - \bar{y}), \\ \bar{y} &= h_2(\bar{x})\bar{x} + k_{21}w(\bar{x}), \end{aligned} \tag{23}$$

where $\bar{x}$ is the estimator state vector and $\bar{y}$ is the estimator output. Usually, the output injection $G(\bar{x})$ has a nonlinear structure; an approximate solution may be derived by using the same procedure based on Taylor's series. Thus, the first order solution is given by, (Isidori and Kang, 1995),

$$(Q - P)G = (K_{21}K_{21}^T)^{-1}(K_{21}G_1^T Q + \gamma^2 H_2^T), \tag{24}$$

where P defines the first-order approximation of the storage function, $V(x) = x^T P x$, for state feedback; Q defines the function $W(\bar{x}) = \bar{x}^T Q \bar{x}$ corresponding to the feedback output problem, while G_1, H_2 and K_{21} are associated to the linearized system (16).

In the case of the ESS, with parameters defined in Table 1, the following output injection is obtained

$$G = \begin{bmatrix} 206.39 \\ 12922.31 \end{bmatrix}, \tag{25}$$

thus leading to the state estimator given in (26)

$$\begin{aligned} \dot{\tilde{x}}_1 &= \tilde{x}_2 - 206.39\tilde{x}_1 + 206.39y, \\ \dot{\tilde{x}}_2 &= 9.8 + \frac{1}{(0.005 + \tilde{x}_1)^2}(-0.000245 - 0.196\tilde{x}_1 \\ &\quad -0.0052\tilde{x}_2) - 12922.3\tilde{x}_1 + 3.26 \cdot 10^{-6}\tilde{x}_2 \\ &\quad +12922.3y. \end{aligned} \tag{26}$$

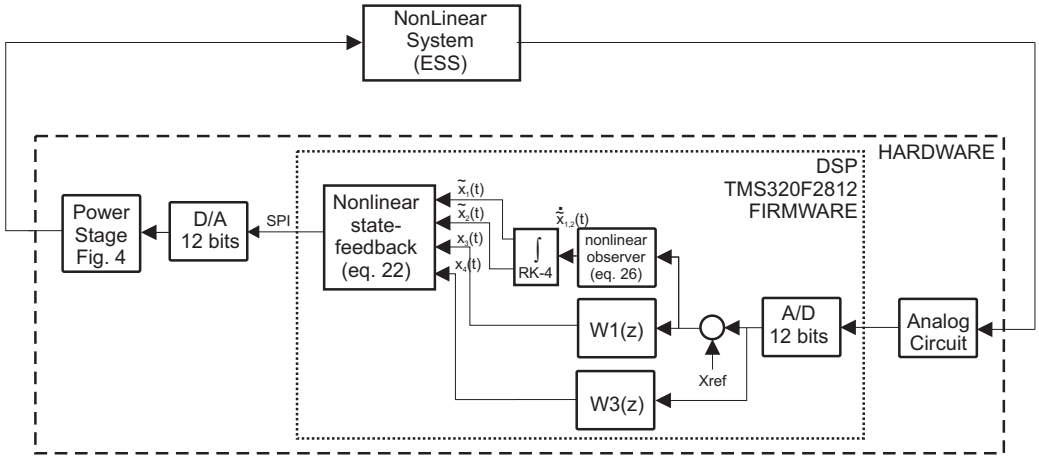

Fig. 3. Output-feedback control configuration

Solutions of these nonlinear equations give the estimated state variables $\tilde{x}_1$ and $\tilde{x}_2$, while x_3 and x_4 are directly given by the realization of W_1 and W_3. The control law (22) makes use of these state variables to implement the output feedback controller.

4. HARDWARE DESCRIPTION

4.1 Control hardware

For the hardware design project, a high performance DSP (TMS320F2812), from Texas Instruments, with 32 bits fixed-point was used. The sampling time was chosen as 200μs for compatibility with the power stage magnetic actuator (f_s = 5kHz). Once dynamic linear weighting functions are being used, *Tustin* bilinear approximation was used to convert continuous-time functions to discrete-time. Due to the nonlinear nature of the observer (26), it is not possible to use the classical linear transformation from continuous time-domain to the discrete-time. So, as in (Sinha and Pechev, 2004), a Runge-Kutta-4 (RK-4) solver was used within the control loop.

Therefore, at every sample of the signal, the control system reads the data from an optical sensor, solves the nonlinear observer equations (26), through RK-4, to estimate $x_1(t)$ and $x_2(t)$, solves the difference equations for $W_1(z)$ and $W_3(z)$ to determine $x_3(t)$ and $x_4(t)$, calculates the control law (22), thus generating the control signal to the power stage that drives the magnetic actuator.

The output-feedback control configuration implemented on the DSP is shown in Fig. 3.

The power stage uses a switched electronic circuit based on a half H-bridge with two MOSFET transistors and two ultrafast recovery diodes, as described in (Shirazee and Basak, 1995), which drives the magnetic coil actuator. The main difference is the coil current and the control voltage signal is injected in a comparator with hysteresis. It can be shown that, in this configuration, the coil current follows the control reference voltage (V_{ref}). Through a PWM control logic electronic circuit, the voltage information created into the comparator element is translated to a pulsed voltage signal that turns the MOSFET transistors ON or OFF. The basic electronic block diagram of the power

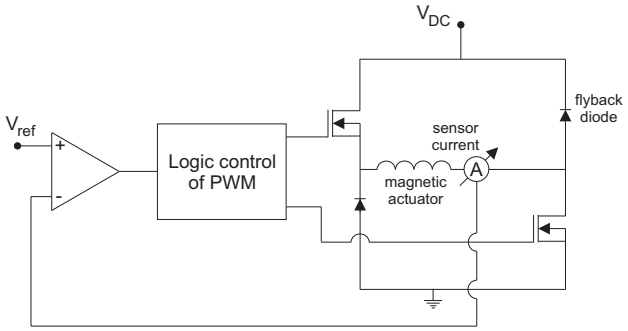

Fig. 4. Block diagram of power circuit stage

stage circuit is given in Fig. 4. This small improvement in the power electronic circuit leads to a linear relationship between the control voltage and the magnet coil current, as expressed in (6) and, as mentioned before, simplifies the mathematical modelling of the ESS.

The digital-analog converter has 12 bits resolution and connects with the DSP by SPI (Serial Peripheral Interface).

4.2 Word-length determination on the fixed-point DSP

Fixed-point digital signal processing is used in many applications due to low cost, high speed and low power consumption. However, most control project designers have used computational tools with floating-point simulation and better numerical resolution (MATLAB/SIMULINK, MAPLE, etc.). As a consequence, in order to implement the controller, designers mostly ride a hard way to adapt the control algorithm for processors with lower numerical resolution on fixed-point.

For this reason, in the last years several optimization techniques have been proposed to translate floating-point algorithms into fixed-point algorithm, without performance degradation (Cantin et al., 2006; Fang et al., 2005; Constantinides et al., 2003). Depending on the application, each technique presents advantages and disadvantages. In this context, manufacturers of computational tools have adapted and made available for the designers practical solutions to minimize this arduous work of translating floating-point algorithm into fixed-point algo-

Table 2. Conversion from MATLAB to ANSI C CODE

MATLAB code using float-point	MATLAB code using fixed-point toolbox	DSP ANSI C code using IQMath library
		`#define GLOBAL_Q 30`
	`IQ=30;`	`#include <IQmathLib.h>`
		`_iq30 aW1,bW1,cW1;`
`aW1=0.002`	`aW1=fi(0.002,1,32,IQ)`	`aW1=_IQ30(0.002);`
`bW1=0.002;`	`bW1=fi(0.002,1,32,IQ);`	`bW1=_IQ30(0.002);`
`cW1=0.9998;`	`bW1=fi(0.9998,1,32,IQ);`	`bW1=_IQ30(0.9998);`
`x3_k=aW1*u1_k+`	`x3_k=fi(fi(aW1*u1_k,1,32,IQ)+`	`x3_k=_IQ30mpyIQX(aW1,30,u1_k,30)+`
`bW1*u1_k_1+`	`fi(bW1*u1_k_1,1,32,IQ)+`	`_IQ30mpyIQX(bW1,30,u1_k,30)+`
`cW1*x3_k;`	`fi(cW1*x3_k_1,1,32,IQ))1,32,IQ);`	`_IQ30mpyIQX(cW1,30,x3_k,30);`
`x3_k_1=x3_k;`	`x3_k_1=x3_k;`	`x3_k_1=x3_k;`
`u1_k_1=u1_k;`	`u1_k_1=u1_k;`	`u1_k_1=u1_k;`
`x=x3_k;`	`x=x3_k.double;`	`x=x3_k;`

rithm, as can be found at Fixed-Point ToolBox in MATLAB/SIMULINK (from MathWorks) and the IQMath Library - A virtual floating point engine (from Texas Instruments). In this section, a practical procedure is presented to make this translation using the Fixed-Point ToolBox in MATLAB and the IQMath Library.

Basically, when the DSP is used for practical implementations, the translation of floating-point algorithm into fixed-point algorithm consists in evaluating the dynamic range and the minimum accuracy of each operand, O_n, in the control algorithm. Thus, it is possible to determine the Integer Word Length (IWL_n) and the Fractional Word Length (FWL_n), where $n = 0, 1, 2, \ldots, N-1$, and where N is the number of operands to be translated. The wordlength for each operand is obtained as follows (Cantin et al., 2006)

$$O_n \rightarrow WL_n = IWL_n + FWL_n + s_i, \tag{27}$$

where the bit $s_i = 1$, if the operand is negative or positive (two's complement arithmetic way); otherwise $s_i = 0$, if the operand is always positive. Thus, after dynamic range verification, all WL_n can be determined for each operand defined in the nonlinear H_∞ control algorithm obtained in section 3.2. Now, with the fi constructor from Fixed-Point Toolbox (MATLAB), it is possible to check, by simulation, if the values of FWL_n and IWL_n for each operand are adequately determined even before the implementation of the DSP firmware (ANSI C Code). The fi constructor accepts value, signedness, wordlength and fraction length (in that order). Example: fi(2.9998, 1, 32, 16) translates the number 2.9998 into fixed-point number with 32 bits of wordlength, 16 bits of fractionlength, 15 bits of integerlength and 1 signed-bit. The IQMath Library (from Texas Instruments) includes a collection of optimized mathematical function for ANSI C Code that can be used directly in mathematical operations (*IQNmpy*, *IQNmpyIQX*, etc.) in the control algorithm (Texas Instruments, 2002). These computational tools can significantly shorten the firmware development time. Table 2 shows small pieces of program CODE to illustrate conversion from MATLAB to ANSI C CODE.

This procedure was very useful during the implementation and debugging stage of the RK-4 algorithm, since the value of the nonlinear observer coefficients differs in many orders of magnitude, (26). Another difficult task in implementing RK-4 algorithm is related to the convergence, which occurred after about 30 steps, each $h = 10^{-4}$ in length.

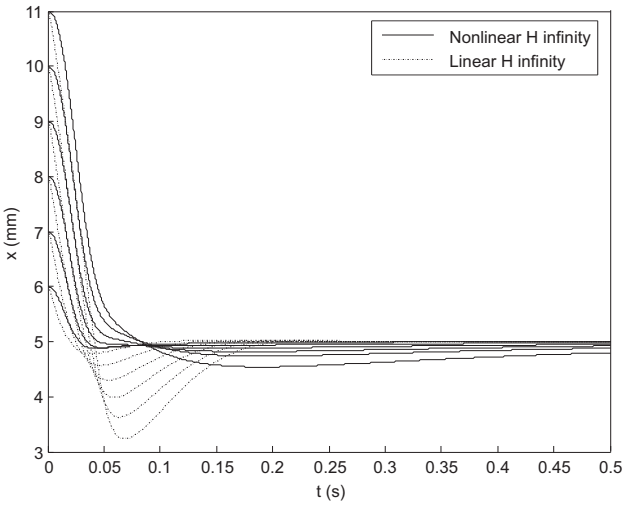

Fig. 5. Simulation results for different gaps

5. EXPERIMENTAL RESULTS

The mechanical setup featured in this work allows selecting different initial gaps. Fig. 5 shows simulations for the linear and nonlinear controllers for different initial gaps. The better performance of the nonlinear controller is evident. In Figs. 6 and 7, it can be seen that experimental results using nonlinear H_∞ control techniques on the DSP are very similar to those obtained by simulation.

The overshoot signal that appears during pull-up was considered acceptable since the rotor did not hit the coil of the actuator and did not fall back.

Another important fact to be considered was the use of optical position sensor that prevented crosstalk between magnetic bearing and sensor. Previous practical experiments conducted by the authors in similar projects showed that the hall sensor presents crosstalk between bearing and sensor, demanding more robustness for the control system

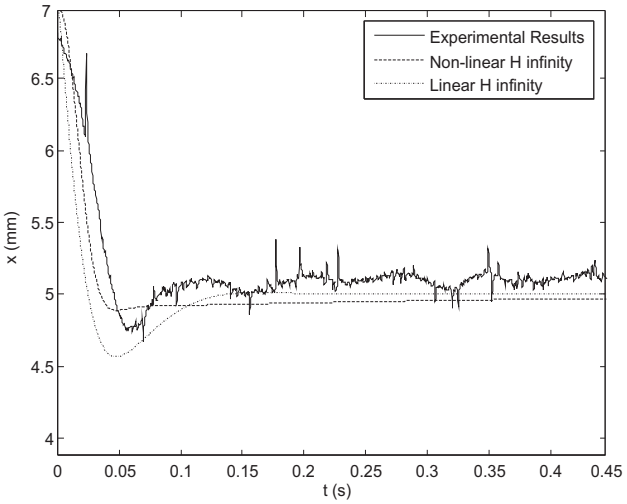

Fig. 6. Experimental results for 7 mm initial gap

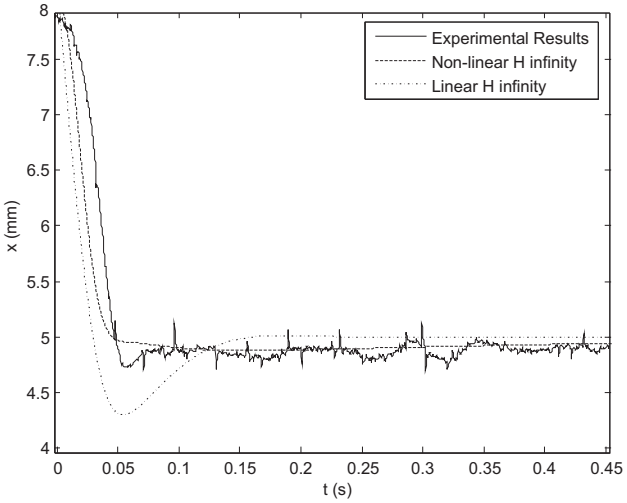

Fig. 7. Experimental results for 8 mm initial gap

if this effect has not been considered in the mathematical modeling.

6. CONCLUSION

This paper described a practical procedure to design a nonlinear H_∞ controller applied to a magnetically levitated system with large initial air-gap. The use of dynamic linear weighting functions in the nonlinear H_∞ control improved the performance and robustness of the ESS. This system was designed and implemented on a fixed-point DSP hardware and tested for large gap operation. The simulations and the experimental results showed that nonlinear H_∞ control was more efficient than that already established linear H_∞ control to solve the instability problem during the initial suspension phase, when the gap is too far from the equilibrium working point.

A practical summarized approach of hardware as well as firmware implementation using MATLAB Fixed-Point Toolbox and IQMath Library that can be easily applied to various discrete-time system realizations with finite wordlength was also described.

ACKNOWLEDGEMENTS

The authors wish to express their thankfulness for the Brazilian Navy – Ministry of Defense.

REFERENCES

N. F. Al-Muthairi and M. Zribi. Sliding mode control of a magnetic levitation system. *Math. Probl. Eng.*, (2): 93–107, 2004.

S. Banerjee, P. Dinkar, and J. Pal. Large gap control in electromagnetic levitation. *ISA Transaction*, (45):215–224, 2006.

A. Bittar and R. M. Sales. H_2 and H_∞ control for maglev vehicles. *IEEE Control System Magazine*, 18:18–25, 1998.

H. Bleuler. A survey of magnetic levitation and magnetic bearing types. *JSME Int. J*, 35:335–342, 1992.

M. A. Cantin, Y. Savaria, D. Prodamos, and P. Lavoie. A metric for automatic word-length determination of hardware datapaths. *IEEE Trans. on Computer-Aided Design of Integrated Circuits and System*, 25(10):2228–2231, 2006.

G. A. Constantinides, P. Y. K. Cheung, and W. Luk. Wordlength optimization for linear digital signal processing. *IEEE Trans. on Computer-Aided Design of Integrated Circuits and System*, 22(10):1432–1442, 2003.

J. C. Doyle, K. Glover, P. P. Khargonekar, and B. A. Francis. State-space solutions to standard H_2 and H_∞ control problems. *IEEE Transactions on Automatic Control*, 34(8):831–847, 1989.

Z. Fang, J. E. Carletta, and R. J. Veillette. A methodology for FPGA-based control implementation. *IEEE Transactions on Control System Technology*, 13(6):977–987, 2005.

A. Isidori and A. Astolfi. Distubance attenuation and H_∞-control via measurement feedback in nonlinear systems. *IEEE Transactions on Automatic Control*, 37(9):1283–1293, 1992.

A. Isidori and W. Kang. H_∞ control via measurement feedback for general nonlinear systems. *IEEE Transactions on Automatic Control*, 40(3):466–472, March 1995.

H. Nadashima. The superconducting magnet for the maglev transport system. *IEEE Trans. Magn.*, 30(6): 1572–1578, 1994.

N. A. Shirazee and A. Basak. Electropernament suspention system for acquiring large air-gaps to suspend loads. *IEEE Trans. Magn.*, 31(6):4193–4195, 1995.

P. K. Sinha. *Electromagnetic Suspension, Dynamics and Control*. Peter Peregrinus Ltd., London, UK, 1987.

P. K. Sinha and A. N. Pechev. Nonlinear H_∞ controllers for electromagnetic suspension systems. *IEEE Transactions on Automatic Control*, 49(4):563–568, 2004.

TI Texas Instruments. *IQMath Library - A Virtual Floating Point Engine*. TI - SPRC87, Dallas, US, 2002.

A. J. van der Schaft. L_2-gain analysis of nonlinear systems and nonlinear state feedback H_∞ control. *IEEE Transactions on Automatic Control*, 37(6):770–784, 1992.